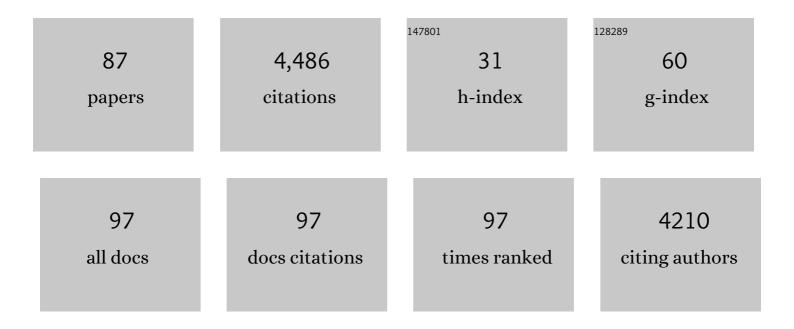
List of Publications by Year in descending order

Source: https://exaly.com/author-pdf/1528378/publications.pdf Version: 2024-02-01



#	Article	IF	CITATIONS
1	Evidence for engagement of the nucleus of the solitary tract in processing intestinal chemonociceptive input irrespective of conscious pain response in healthy humans. Pain, 2022, 163, 1520-1529.	4.2	7
2	Concurrent CBF and BOLD fMRI with dual-echo spiral simultaneous multi-slice acquisitions at 7T. NeuroImage, 2022, 247, 118820.	4.2	5
3	Worry Modifies the Relationship between Locus Coeruleus Activity and Emotional Mnemonic Discrimination. Brain Sciences, 2022, 12, 381.	2.3	0
4	<scp>BUDAâ€MESMERISE</scp> : Rapid acquisition and unsupervised parameter estimation for <scp>T₁</scp> , <scp>T₂</scp> , <scp>M₀</scp> , <scp>B₀</scp> , and <scp>B₁</scp> maps. Magnetic Resonance in Medicine, 2022, 88, 292-308.	3.0	4
5	Highly accelerated <scp>EPI</scp> with wave encoding and multiâ€shot simultaneous multislice imaging. Magnetic Resonance in Medicine, 2022, 88, 1180-1197.	3.0	3
6	Magnetic field strength dependent SNR gain at the center of a spherical phantom and up to 11. <scp>7T</scp> . Magnetic Resonance in Medicine, 2022, 88, 2131-2138.	3.0	21
7	Layer-dependent functional connectivity methods. Progress in Neurobiology, 2021, 207, 101835.	5.7	67
8	Sub-millimetre resolution laminar fMRI using Arterial Spin Labelling in humans at 7 T. PLoS ONE, 2021, 16, e0250504.	2.5	27
9	7T dynamic contrastâ€enhanced MRI for the detection of subtle blood–brain barrier leakage. Journal of Neuroimaging, 2021, 31, 902-911.	2.0	7
10	LayNii: A software suite for layer-fMRI. NeuroImage, 2021, 237, 118091.	4.2	64
11	Validating layer-specific VASO across species. Neurolmage, 2021, 237, 118195.	4.2	11
12	Magnetization transfer weighted EPI facilitates cortical depth determination in native fMRI space. NeuroImage, 2021, 242, 118455.	4.2	4
13	Temporal SNR optimization through RF coil combination in fMRI: The more, the better?. PLoS ONE, 2021, 16, e0259592.	2.5	1
14	Integrated VASO and perfusion contrast: A new tool for laminar functional MRI. NeuroImage, 2020, 207, 116358.	4.2	35
15	Sub-millimeter fMRI reveals multiple topographical digit representations that form action maps in human motor cortex. NeuroImage, 2020, 208, 116463.	4.2	88
16	Application of Evolution Strategies to the Design of SAR Efficient Parallel Transmit Multi-Spoke Pulses for Ultra-High Field MRI. IEEE Transactions on Medical Imaging, 2020, 39, 4225-4236.	8.9	5
17	Transcutaneous vagus nerve stimulation increases locus coeruleus function and memory performance in older individuals. Alzheimer's and Dementia, 2020, 16, e044766.	0.8	4
18	Rostroâ€caudal locus coeruleus integrity differences vary with age and sex using ultraâ€high field imaging. Alzheimer's and Dementia, 2020, 16, e046722.	0.8	1

#	Article	IF	CITATIONS
19	Unraveling the contributions to the neuromelanin-MRI contrast. Brain Structure and Function, 2020, 225, 2757-2774.	2.3	41
20	Dynamic behavior of the locus coeruleus during arousal-related memory processing in a multi-modal 7T fMRI paradigm. ELife, 2020, 9, .	6.0	43
21	In vivo imaging of the nucleus of the solitary tract with Magnetization Transfer at 7 Tesla. NeuroImage, 2019, 201, 116071.	4.2	16
22	Locus coeruleus imaging as a biomarker for noradrenergic dysfunction in neurodegenerative diseases. Brain, 2019, 142, 2558-2571.	7.6	219
23	The potential of MR-Encephalography for BCI/Neurofeedback applications with high temporal resolution. NeuroImage, 2019, 194, 228-243.	4.2	14
24	Optimizing BOLD sensitivity in the 7T Human Connectome Project resting-state fMRI protocol using plug-and-play parallel transmission. NeuroImage, 2019, 195, 1-10.	4.2	18
25	The influence of spatial resolution on the spectral quality and quantification accuracy of wholeâ€brain MRSI at 1.5T, 3T, 7T, and 9.4T. Magnetic Resonance in Medicine, 2019, 82, 551-565.	3.0	22
26	Minimal Linear Networks for Magnetic Resonance Image Reconstruction. Scientific Reports, 2019, 9, 19527.	3.3	8
27	Comparison of SMS-EPI and 3D-EPI at 7T in an fMRI localizer study with matched spatiotemporal resolution and homogenized excitation profiles. PLoS ONE, 2019, 14, e0225286.	2.5	24
28	Frequency-specific attentional modulation in human primary auditory cortex and midbrain. NeuroImage, 2018, 174, 274-287.	4.2	11
29	Techniques for blood volume fMRI with VASO: From low-resolution mapping towards sub-millimeter layer-dependent applications. NeuroImage, 2018, 164, 131-143.	4.2	101
30	A method for the dynamic correction of B 0 -related distortions in single-echo EPI at 7 T. NeuroImage, 2018, 168, 321-331.	4.2	57
31	Impact of acquisition and analysis strategies on cortical depth-dependent fMRI. NeuroImage, 2018, 168, 332-344.	4.2	71
32	Pulse sequences and parallel imaging for high spatiotemporal resolution MRI at ultra-high field. NeuroImage, 2018, 168, 101-118.	4.2	47
33	High-resolution in vivo imaging of human locus coeruleus by magnetization transfer MRI at 3T and 7T. NeuroImage, 2018, 168, 427-436.	4.2	104
34	Resolving laminar activation in human V1 using ultra-high spatial resolution fMRI at 7T. Scientific Reports, 2018, 8, 17063.	3.3	53
35	Ultra-high resolution blood volume fMRI and BOLD fMRI in humans at 9.4†T: Capabilities and challenges. NeuroImage, 2018, 178, 769-779.	4.2	44
36	Using multi-echo simultaneous multi-slice (SMS) EPI to improve functional MRI of the subcortical nuclei of the basal ganglia at ultra-high field (7T). NeuroImage, 2018, 172, 886-895.	4.2	32

#	Article	IF	CITATIONS
37	inhomogeneity mitigation in CEST using parallel transmission. Magnetic Resonance in Medicine, 2017, 78, 2216-2225.	3.0	18
38	Optimization of simultaneous multislice EPI for concurrent functional perfusion and BOLD signal measurements at 7T. Magnetic Resonance in Medicine, 2017, 78, C1-C1.	3.0	0
39	Comparison of 3 T and 7 T ASL techniques for concurrent functional perfusion and BOLD studies. NeuroImage, 2017, 156, 363-376.	4.2	34
40	Multi-echo fMRI: A review of applications in fMRI denoising and analysis of BOLD signals. NeuroImage, 2017, 154, 59-80.	4.2	238
41	Estimating and eliminating the excitation errors in bipolar gradient composite excitations caused by radiofrequencyâ€gradient delay: Example of bipolar spokes pulses in parallel transmission. Magnetic Resonance in Medicine, 2017, 78, 1883-1890.	3.0	11
42	Rapid whole-brain resting-state fMRI at 3ÂT: Efficiency-optimized three-dimensional EPI versus repetition time-matched simultaneous-multi-slice EPI. NeuroImage, 2017, 163, 81-92.	4.2	39
43	Echo-time dependence of the BOLD response transients – A window into brain functional physiology. NeuroImage, 2017, 159, 355-370.	4.2	23
44	Highâ€resolution gradientâ€recalled echo imaging at 9.4T using 16â€channel parallel transmit simultaneous multislice spokes excitations with sliceâ€byâ€slice flip angle homogenization. Magnetic Resonance in Medicine, 2017, 78, 1050-1058.	3.0	22
45	High-Resolution CBV-fMRI Allows Mapping of Laminar Activity and Connectivity of Cortical Input and Output in Human M1. Neuron, 2017, 96, 1253-1263.e7.	8.1	255
46	Variable slice thickness (VAST) EPI for the reduction of susceptibility artifacts in whole-brain GE-EPI at 7 Tesla. Magnetic Resonance Materials in Physics, Biology, and Medicine, 2017, 30, 591-607.	2.0	4
47	Optimization of simultaneous multislice EPI for concurrent functional perfusion and BOLD signal measurements at 7T. Magnetic Resonance in Medicine, 2017, 78, 121-129.	3.0	24
48	Functional cerebral blood volume mapping with simultaneous multi-slice acquisition. NeuroImage, 2016, 125, 1159-1168.	4.2	22
49	Correcting dynamic distortions in 7T echo planar imaging using a jittered echo time sequence. Magnetic Resonance in Medicine, 2016, 76, 1388-1399.	3.0	20
50	Simultaneous multislice (SMS) imaging techniques. Magnetic Resonance in Medicine, 2016, 75, 63-81.	3.0	420
51	High-resolution diffusion MRI at 7T using a three-dimensional multi-slab acquisition. NeuroImage, 2016, 143, 1-14.	4.2	55
52	Volumetric imaging with homogenised excitation and static field at 9.4 T. Magnetic Resonance Materials in Physics, Biology, and Medicine, 2016, 29, 333-345.	2.0	23
53	The quest for the best: The impact of different EPI sequences on the sensitivity of random effect fMRI group analyses. NeuroImage, 2016, 126, 49-59.	4.2	55
54	A Specialized Multi-Transmit Head Coil for High Resolution fMRI of the Human Visual Cortex at 7T. PLoS ONE, 2016, 11, e0165418.	2.5	23

#	Article	IF	CITATIONS
55	<scp>SENSE</scp> and simultaneous multislice imaging. Magnetic Resonance in Medicine, 2015, 74, 1356-1362.	3.0	57
56	Design of parallel transmission pulses for simultaneous multislice with explicit control for peak power and local specific absorption rate. Magnetic Resonance in Medicine, 2015, 73, 1946-1953.	3.0	51
57	lterative projection onto convex sets for quantitative susceptibility mapping. Magnetic Resonance in Medicine, 2015, 73, 697-703.	3.0	3
58	RF peak power reduction in CAIPIRINHA excitation by interslice phase optimization. NMR in Biomedicine, 2015, 28, 1393-1401.	2.8	6
59	Sub-millimeter T2 weighted fMRI at 7 T: comparison of 3D-GRASE and 2D SE-EPI. Frontiers in Neuroscience, 2015, 9, 163.	2.8	70
60	Simultaneous acquisition of cerebral blood volumeâ€, blood flowâ€, and blood oxygenationâ€weighted <scp>MRI</scp> signals at ultraâ€high magnetic field. Magnetic Resonance in Medicine, 2015, 74, 513-517.	3.0	9
61	Fast quantitative susceptibility mapping using 3D EPI and total generalized variation. NeuroImage, 2015, 111, 622-630.	4.2	157
62	BOLD fMRI signal characteristics of S1- and S2-SSFP at 7 Tesla. Frontiers in Neuroscience, 2014, 8, 49.	2.8	21
63	A study-specific fMRI normalization approach that operates directly on high resolution functional EPI data at 7Tesla. NeuroImage, 2014, 100, 710-714.	4.2	18
64	Simultaneous multislice spectralâ€spatial excitations for reduced signal loss susceptibility artifact in BOLD functional MRI. Magnetic Resonance in Medicine, 2014, 72, 1342-1352.	3.0	8
65	Slab-selective, BOLD-corrected VASO at 7 Tesla provides measures of cerebral blood volume reactivity with high signal-to-noise ratio. Magnetic Resonance in Medicine, 2014, 72, 137-148.	3.0	107
66	Threeâ€dimensional Fourier encoding of simultaneously excited slices: Generalized acquisition and reconstruction framework. Magnetic Resonance in Medicine, 2014, 71, 2071-2081.	3.0	58
67	Prevention of motionâ€induced signal loss in diffusionâ€weighted echoâ€planar imaging by dynamic restoration of gradient moments. Magnetic Resonance in Medicine, 2014, 71, 2006-2013.	3.0	22
68	Simultaneous Multi-Slice fMRI using spiral trajectories. NeuroImage, 2014, 92, 8-18.	4.2	30
69	Phonological markers of information structure: An fMRI study. Neuropsychologia, 2014, 58, 64-74.	1.6	9
70	Simultaneous multislice excitation by parallel transmission. Magnetic Resonance in Medicine, 2014, 71, 1416-1427.	3.0	51
71	Singleâ€shot echoâ€planar imaging with Nyquist ghost compensation: Interleaved dual echo with acceleration (IDEA) echoâ€planar imaging (EPI). Magnetic Resonance in Medicine, 2013, 69, 37-47.	3.0	23
72	Modeling and suppression of respiration induced B0-fluctuations in non-balanced steady-state free precession sequences at 7 Tesla. Magnetic Resonance Materials in Physics, Biology, and Medicine, 2013, 26, 377-387.	2.0	2

#	Article	IF	CITATIONS
73	Memoryâ€Related Hippocampal Activity Can Be Measured Robustly Using fMRI at 7 Tesla. Journal of Neuroimaging, 2013, 23, 445-451.	2.0	23
74	Timeâ€interleaved acquisition of modes: An analysis of SAR and image contrast implications. Magnetic Resonance in Medicine, 2012, 67, 1033-1041.	3.0	30
75	Referenceâ€free unwarping of EPI data using dynamic offâ€resonance correction with multiecho acquisition (DOCMA). Magnetic Resonance in Medicine, 2012, 68, 1247-1254.	3.0	32
76	Spectral decomposition of susceptibility artifacts for spectralâ€spatial radiofrequency pulse design. Magnetic Resonance in Medicine, 2012, 68, 1905-1910.	3.0	6
77	Exploring the postâ€stimulus undershoot with spinâ€echo fMRI: Implications for models of neurovascular response. Human Brain Mapping, 2011, 32, 141-153.	3.6	15
78	Application of wholeâ€brain CBVâ€weighted fMRI to a cognitive stimulation paradigm: Robust activation detection in a stroop task experiment using 3D GRASE VASO. Human Brain Mapping, 2011, 32, 974-981.	3.6	22
79	Advances in High-Field BOLD fMRI. Materials, 2011, 4, 1941-1955.	2.9	21
80	RF excitation using time interleaved acquisition of modes (TIAMO) to address <i>B</i> ₁ inhomogeneity in highâ€field MRI. Magnetic Resonance in Medicine, 2010, 64, 327-333.	3.0	115
81	Three dimensional echo-planar imaging at 7 Tesla. NeuroImage, 2010, 51, 261-266.	4.2	266
82	3D singleâ€ s hot VASO using a maxwell gradient compensated GRASE sequence. Magnetic Resonance in Medicine, 2009, 62, 255-262.	3.0	34
83	A dual echo approach to removing motion artefacts in fMRI time series. NMR in Biomedicine, 2009, 22, 551-560.	2.8	33
84	Investigating the benefits of multi-echo EPI for fMRI at 7ÂT. NeuroImage, 2009, 45, 1162-1172.	4.2	121
85	Fast spin echo sequences for BOLD functional MRI. Magnetic Resonance Materials in Physics, Biology, and Medicine, 2007, 20, 11-17.	2.0	59
86	Measurement of activation-related changes in cerebral blood volume: VASO with single-shot HASTE acquisition. Magnetic Resonance Materials in Physics, Biology, and Medicine, 2007, 20, 63-67.	2.0	22
87	BOLD contrast sensitivity enhancement and artifact reduction with multiecho EPI: Parallel-acquired inhomogeneity-desensitized fMRI. Magnetic Resonance in Medicine, 2006, 55, 1227-1235.	3.0	399